

# Unbinding Pathways of VEGFR2 Inhibitors Revealed by Steered Molecular Dynamics

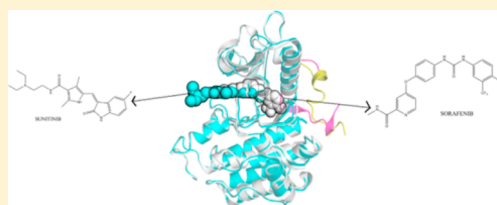
Anna Maria Capelli<sup>†,‡</sup> and Gabriele Costantino<sup>\*‡</sup>

<sup>†</sup>Chemistry Research and Drug Design Department, Chiesi Farmaceutici S.p.A., Largo F. Belloli 11a, 43122 Parma, Italy

<sup>‡</sup>Dipartimento di Farmacia, Università degli Studi di Parma, Viale Area delle Scienze 27/A, 43100 Parma, Italy

## S Supporting Information

**ABSTRACT:** A detailed atomistic description of the unbinding process of sorafenib and sunitinib, two known VEGFR2 inhibitors clinically used to treat renal cell carcinoma, was unraveled by using steered molecular dynamics (SMD) simulations. While sunitinib is a fast-dissociating binder, sorafenib exhibits quite a long residence time at this enzyme, which might impact its duration of action *in vivo*. In order to gain insights into the kinetically different behaviors of the two inhibitors, an SMD study was carried out, which involved a careful optimization of the force and velocity parameters. We were able to identify two different binding pathways for the two inhibitors, as sunitinib exited the ATP binding site from the cavity entrance without a rupture point while sorafenib moved opposite to the ATP binding site entrance. Furthermore, the calculated  $\Delta G_{\text{off}}$  values clearly reflect on a qualitative level the distinct off-rates of the two inhibitors, thus suggesting that this protocol could be tried on other VEGFR2 ligands to assess its robustness and then used to rank structural analogues of these derivatives.



## INTRODUCTION

In the early phase of drug discovery, medicinal chemistry efforts are mainly aimed at the optimization of both *in vitro* and *in vivo* profiles of drug candidates. For this purpose, several techniques have been developed and are routinely used to model and predict *in silico* drug–target affinity and selectivity indexes. On the contrary, the prediction of the duration of drug efficacy *in vivo* is still elusive. This complex property depends on the rate constant for receptor–ligand association (the on-rate,  $k_{\text{on}}$ ) and, most critically, on the dissociation rate constant (the off-rate,  $k_{\text{off}}$ ), which in turn can be translated into a dissociative half-life ( $t_{1/2}$ ) for the receptor–ligand complex as a direct measure of residence time.<sup>1</sup> In view of the fact that the duration of drug efficacy *in vivo* is key to lead optimization, the availability of robust computational approaches that can qualitatively predict or rank derivatives according to their residence times at a target would accelerate candidate selection. Among the methods that have been proposed to model ligand–receptor unbinding pathways, steered molecular dynamics (SMD) is becoming popular in light of its theoretical simplicity, reproducibility, and relatively low computational cost.<sup>2–9</sup> SMD consists of pulling a molecule out of its receptor binding pocket by applying a guiding potential along a reaction coordinate with constant force and velocity. Hence, this enhanced-sampling approach accelerates ligand unbinding, and upon fulfillment of the stiff-spring approximation as well as application of the Jarzynski equality<sup>10</sup> to replicated trajectories, the potential of mean force (PMF) can be reconstructed and the free energy calculated for a nonequilibrium process. In particular, the simulation of the unbinding trajectory of a ligand from its binding pocket yields a value of  $\Delta G_{\text{off}}$ , which is related to the

experimental unbinding off-rate constant at least for a congeneric compound series ( $k_{\text{off}} \propto 1/\Delta G_{\text{off}}$ ). More importantly, atomistic details of the unbinding process can be inferred from SMD trajectories, which is instrumental for drug design purposes. Despite its theoretical simplicity, SMD depends on some critical parameters that need careful calibration for each case study, in particular the pulling velocity, force constant, and reaction coordinate. In principle, the pulling velocity should be very low to ensure that the system under study can satisfy a quasi-static approximation. In practice this is counterbalanced by the calculation time, which depends on the power of the computational infrastructure used to accomplish these simulations. Furthermore, the force constant has to be stiff enough to allow the system to follow the guiding potential. However, Park and co-workers<sup>11,12</sup> have reported that the use of a very stiff force constant can lead to severe distortions of the system under study. Besides, the Jarzynski equality has been developed for canonical systems to derive Helmholtz rather than Gibbs free energy and requires that SMD simulations be replicated on different snapshots of a pre-equilibrated system in order to get statistically significant results. However, the most critical parameter is still represented by the selection of the unbinding reaction coordinate along which the ligand leaves the binding site.

Herein we report the application of SMD to elucidate the unbinding pathways of two drugs from the human vascular endothelial growth factor receptor 2 (VEGFR2), a clinically validated target implicated in renal cell carcinoma (RCC).<sup>13</sup>

Received: July 4, 2014



ACS Publications

© XXXX American Chemical Society

A

dx.doi.org/10.1021/ci500527j | J. Chem. Inf. Model. XXXX, XXX, XXX–XXX

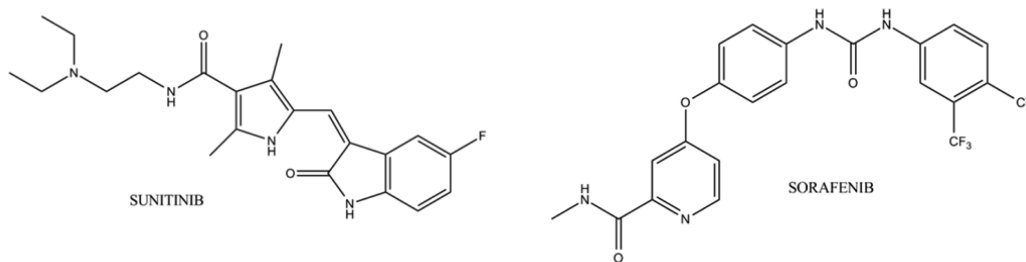


**Figure 1.** Chemical structures of (left) sunitinib (Sutent) and (right) sorafenib (Nexavar).

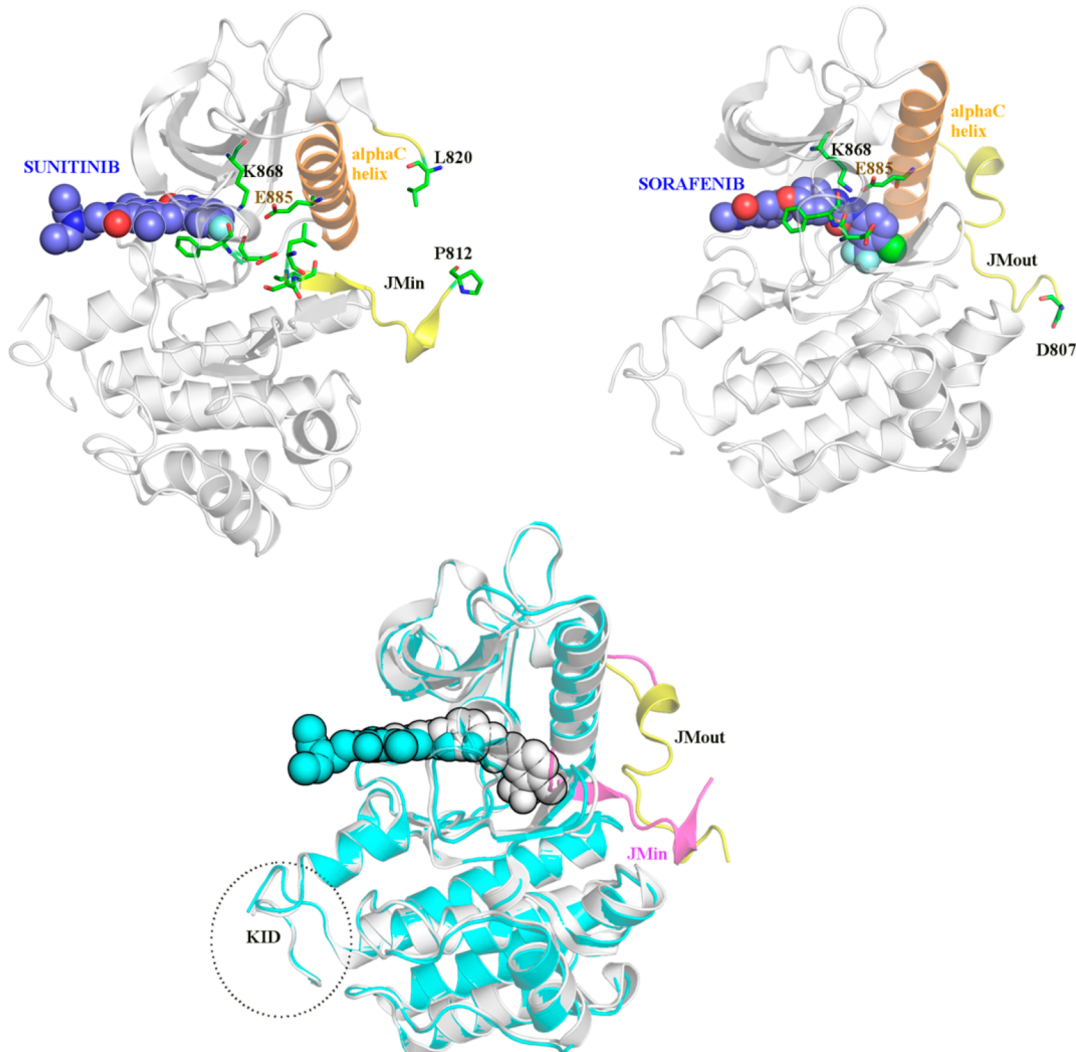


**Figure 2.** (top left) Overview of the crystal complex of sunitinib bound to the catalytic and JM domains of human VEGFR2 (VEGFR2/SUN, PDB code 4AGD). This picture highlights the close proximity of I804 in the JM domain to the ATP binding site where the inhibitor binds. The JM domain has not been solved between P812 and L820. (top right) Overview of the crystal complex of sorafenib with the catalytic and JM domains of human VEGFR2 (VEGFR2/SOR, PDB code 4ASD). The JM domain, which has not been solved between L802 and M806, is away from the ATP binding site and the ligand locked in the binding site. (bottom center) Overlay of the sorafenib (cyan) and sunitinib (gray) crystal complexes. As shown, sorafenib binds deeper in the binding site with respect to sunitinib and changes the JM domain from the “in” conformation (JM<sub>in</sub>, yellow) to the “out” conformation (JM<sub>out</sub>, blue).

VEGFR2 is a type-III receptor tyrosine kinase (RTK) whose 7-immunoglobulin-like extracellular domain is connected to the intracellular kinase catalytic domain (CD) through the transmembrane (TM) domain embedded in the phospholipid bilayer and a stretch of amino acids known as the juxtamembrane domain (JM).

Recently the crystal structures of two clinically relevant tyrosine kinase inhibitors, namely, sunitinib and sorafenib (Figure 1), bound to the unphosphorylated kinase domain and to the JM domain of VEGFR2 have been solved.<sup>14</sup> As shown in Figure 2 (top left), in the sunitinib complex (VEGFR2/SUN, PDB code 4AGD) the N-terminus portion of the JM domain is packed close to the DFG motif and to the ATP binding site

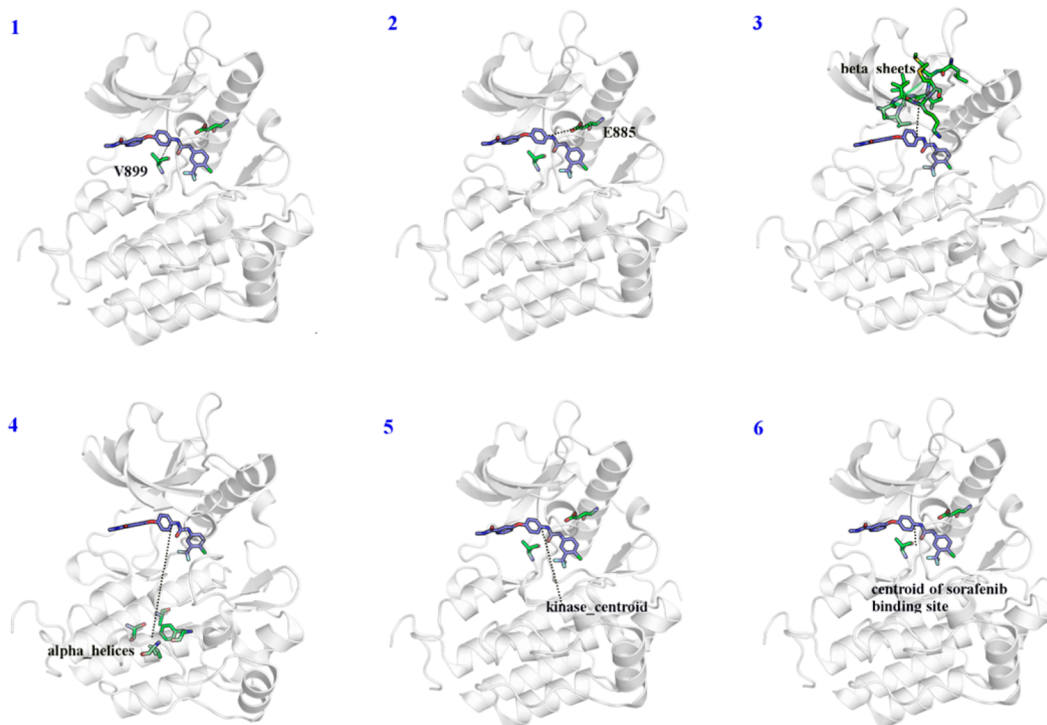


**Figure 3.** Overview of the trajectories explored.

(the “in” conformation), preventing the activation loop transition from the DFG-out to the DGF-in conformation needed to bind ATP. On the contrary, sorafenib (VEGFR2/SOR, PDB code 4ASD) binds deeper in the VEGFR2 ATP binding site (Figure 2, top right); the DFG-triad still adopts the “out” conformation, but the JM domain is oriented away from the DFG motif ( $JM_{out}$ ). As shown in Figure 2 (bottom), the overlay of sorafenib and sunitinib bound to the kinase domain of VEGFR2 emphasizes how the former inhibitor binds deeper in the ATP binding site than the latter, leading to a dramatic change in the conformation of the JM domain only. Medicinal chemistry investigations and modeling studies of sunitinib and some close analogues have recently been reported in the literature.<sup>15,16</sup>

The different binding modes of the two inhibitors are reflected by their quite different residence times at VEGFR2.<sup>17</sup> While sunitinib is a prototypical type-IV inhibitor, showing a short half-life for dissociation from VEGFR2 ( $t_{1/2} \approx 5$  min),<sup>17</sup> sorafenib is an exemplar of a type-II inhibitor characterized by long half-life for dissociation from VEGFR2 ( $t_{1/2} = 340$  min).<sup>17</sup> Because of their different kinetic profiles, sorafenib and sunitinib were selected as suitable prototypes to calibrate the SMD parameters and assess the performance of this methodology in predicting their off-rates. Besides, atomistic details of their unbinding pathways were collected in order to gather insights for drug-design purposes.

## METHODS

**Protein Preparation.** 3D coordinates of the crystal structure of sunitinib bound to the inactivated catalytic domain of the human VEGFR2, solved together with the juxtamembrane domain, were retrieved from the Protein Data Bank (PDB code 4AGD,  $JM_{in}$ ). Five alanine residues were introduced to join Y938 to Y996, corresponding to the kinase insert domain (KID), which plays a structural role by connecting two

$\alpha$  helices in the C-terminus CD. This loop had been deleted for crystallization purposes without affecting the intrinsic kinase activity. Furthermore, amino acids 813–819 in the JM domain, which were not solved in the X-ray structure, were manually added within Maestro v9.1.<sup>18</sup> Subsequently, these fragments were gently relaxed with OPLS\_2005 FF (minimization task, PRCG minimization method, Maestro v9.1) while keeping the rest of the protein fixed. All of the water molecules present in the X-ray structure were removed. Sunitinib was modeled starting from its crystallographic coordinates (VEGFR2/SUN).

The crystal structure of human VEGFR2 (juxtamembrane and catalytic domains) in complex with sorafenib was retrieved from the Protein Data Bank (PDB code 4ASD,  $JM_{out}$ ). As for the sunitinib complex, five alanine residues were added to bridge Y938 to Y996. Besides, amino acids 802–806 in the N-terminus domain, which were not solved in the X-ray structure, were manually added within Maestro v9.1 in an extended conformation and away from the catalytic domain. Then the added amino acids were gently minimized with OPLS\_2005 FF as above while keeping the rest of the protein fixed. All of the water molecules present in the X-ray complex were removed. Sorafenib was modeled starting from its crystallographic coordinates (VEGFR2/SOR). Following this preparation, both complexes had the same number of atoms.

**Ligand Preparation.** The geometries of the sorafenib and sunitinib structures were optimized using the Jaguar tool available in Maestro v9.1, and partial charges were computed at the HF/6-31G\*\* level of theory and fixed using the RESP methodology. Atom types and ligand parameters were assigned using the general Amber force field (gaff).<sup>19</sup>

**Preparation of Ligand–Receptor Complexes.** Each ligand–receptor construct was finally parametrized using the amber99SB and gaff force fields.<sup>19</sup> The complexes thus obtained were solvated with TIP3P water models in a 12 Å

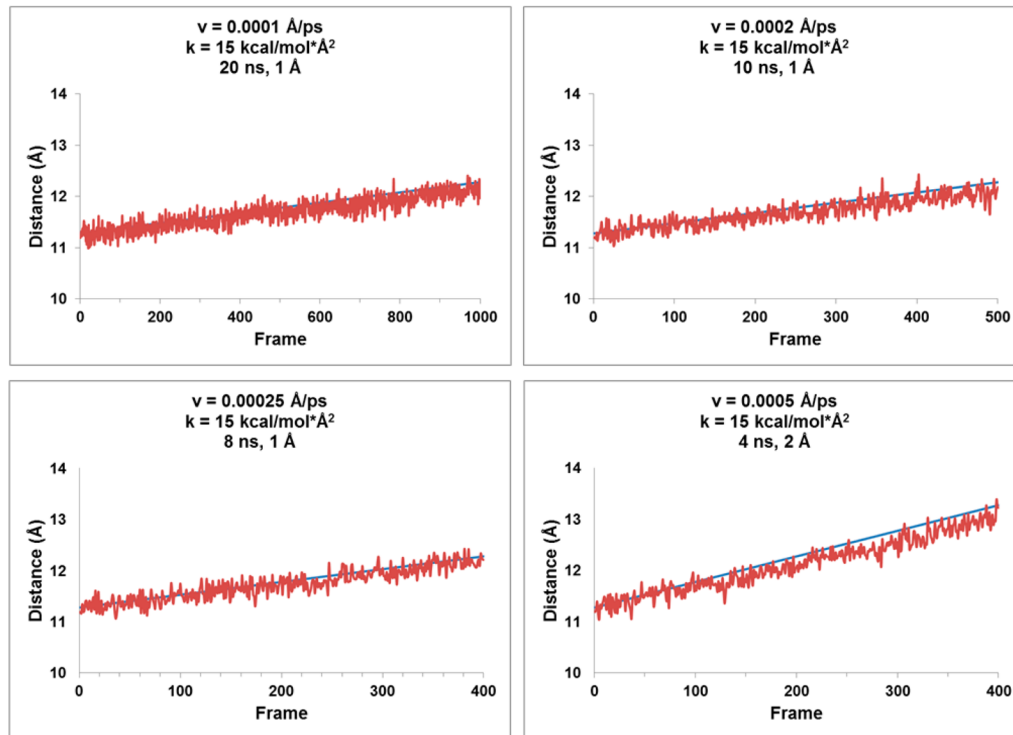


**Figure 4.** Plots of the end-to-end distance (red line) and the constrained distance (blue line) (Y axis) measured in each frame (X axis) in simulations of the VEGFR2/SUN complex performed with  $k = 15 \text{ kcal mol}^{-1} \text{ \AA}^{-2}$  and  $v = 0.0001, 0.0002, 0.00025$ , and  $0.0005 \text{ \AA}/\text{ps}$ .

cubic box using Leap, and  $\text{Na}^+$  ions were added to neutralize the net charge of the system.

**MD Simulation Parameters and Protocols.** All of the MD simulations were performed with Amber 11.<sup>19</sup> All of the systems were gradually minimized and then equilibrated for 0.5 ns. During each equilibration phase, the *NPT* ensemble was used with a pressure target equal to 1 atm, a temperature of 310 K, a pressure relaxation time of 1 ps, and a collision frequency set to  $5 \text{ ps}^{-1}$ . The cutoff for nonbonded interactions was set to 10 Å, and the particle mesh Ewald algorithm was used with a grid spacing of 1 Å. A two-step equilibration procedure was used. Each step lasted for 0.25 ns with an integration step of 1 fs. The first 0.25 ns step of the equilibration was conducted by imposing harmonic constraints equal to  $2 \text{ kcal mol}^{-1} \text{ \AA}^{-2}$  on the protein backbone and the ligand atoms. For the second 0.25 ns step, the same MD conditions were used, and the constraints on the ligand atoms were set to  $2 \text{ kcal mol}^{-1} \text{ \AA}^{-2}$ . Finally a production run was conducted for a total of 20 ns for each system. The first 10 ns was done using the *NPT* ensemble, while for the last 10 ns the *NVT* ensemble was used in order to prepare the systems for the following SMD runs. During the production phase, the integration step was set equal to 2 fs and only bonds involving hydrogen atoms were constrained. The MD conditions were kept the same as those used for the equilibration phase, without imposing any harmonic constraints on the system. Along the last 5 ns of the *NVT* production phase (5000 frames) for each complex, some frames (four for sunitinib, five for sorafenib) were randomly taken and used for constant-velocity SMD (*NVT* ensemble, Amber 12).<sup>19</sup>

**Calibration of the SMD Simulation Parameters.** Both the constant velocity ( $v$ ) and the force constant ( $k$ ) were identified using the following stepwise optimization: (i) SMD simulations were conducted on the last sampled frames of the *NVT* trajectories of the VEGFR2/SUN (fast-dissociating

ligand) and VEGFR2/SOR (slow-dissociating ligand) complexes by setting  $v$  to 0.0001, 0.0002, 0.00025, and 0.0005 Å/ps while keeping  $k$  fixed at  $15 \text{ kcal mol}^{-1} \text{ \AA}^{-2}$ ; (ii) SMD simulations were conducted on both of the complexes by setting  $k$  to 5, 10, 15, 20, 30, and 40 kcal mol $^{-1}$  Å $^{-2}$  while keeping  $v$  fixed at 0.0005 Å/ps; (iii) selection of the smallest  $k$  and  $v$  that allow for the conservation of the stiff-spring approximation for both the systems ( $v = 0.0005 \text{ \AA}/\text{ps}$ ,  $k = 40 \text{ kcal mol}^{-1} \text{ \AA}^{-2}$ ).

The unbinding reaction coordinate was identified upon visual inspection of the crystal structures, and the following trials were performed on representative frames of both complexes:

1. the distance between the ligand center of mass and the C $\alpha$  atom of V899 (Figure 3, panel 1);
2. the distance between the ligand center of mass and the C $\alpha$  atom of E885 (Figure 3, panel 2);
3. the distance between the ligand center of mass and the centroid of the C $\alpha$  atoms of A866–M869 and L912–V916 (N-lobe  $\beta$ -sheets; Figure 3, panel 3);
4. the distance between the ligand center of mass and the centroid of the C $\alpha$  atoms of S1009, A1013, F1091, and L1095 (C-lobe  $\alpha$ -helices; Figure 3, panel 4);
5. the distance between the ligand center of mass and the centroid of the whole kinase (Figure 3, panel 5);
6. the distance between the ligand center of mass and the sorafenib binding site center of mass (C $\alpha$  atoms; Figure 3, panel 6).

The root-mean-square deviation (RMSD) of the protein trace of each sampled frame was calculated within VMD<sup>20</sup> to monitor kinase conformational changes.

All of these Amber experiments were run on Cineca Consortium Europa CPUs (64 processors) and lasted for 12 h/processor for  $v = 0.0005 \text{ \AA}/\text{ps}$  and  $k = 40 \text{ kcal mol}^{-1} \text{ \AA}^{-2}$  and

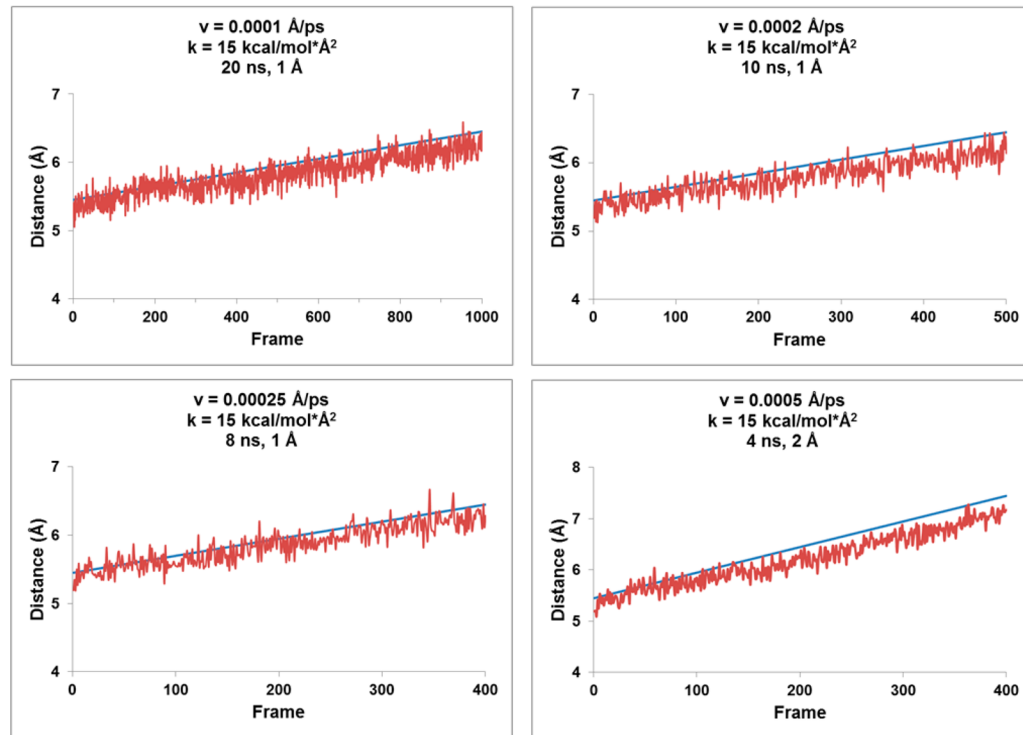


**Figure 5.** Plots of the end-to-end distance (red line) and the constrained distance (blue line) (Y axis) measured in each frame (X axis) in simulations of the VEGFR2/SOR complex performed with  $k = 15 \text{ kcal mol}^{-1} \text{ \AA}^{-2}$  and  $v = 0.0001, 0.0002, 0.00025$ , and  $0.0005 \text{ \AA/ps}$ .

for 25 h/processor for  $v = 0.0001 \text{ \AA/ps}$  and  $k = 15 \text{ kcal mol}^{-1} \text{ \AA}^{-2}$ .

**Calculation of the Potential of Mean Force.** All five selected frames of the equilibrated sorafenib complex were used as starting structures for displacement by 20 Å along the reaction coordinate, defined as the distance between the ligand center of mass and the centroid of the sorafenib binding site. Four representative frames of the equilibrated sunitinib complex were utilized as starting structures for displacement by 12 Å along the reaction coordinate. After displacement by 10 Å, the ligand lies outside the ATP binding site. All of the SMD runs were conducted by imposing a pulling velocity of  $v = 0.0005 \text{ \AA/ps}$  and with a force constant of  $k = 40 \text{ kcal mol}^{-1} \text{ \AA}^{-2}$ . The value of the exerted force ( $F_{\text{ex}}$ ) was printed out every 5 ps (dt), and the work done on the system ( $W$ ) during SMD was calculated by numerical integration (eq 1,  $\text{dx} = v \text{ dt}$ ).<sup>6–8</sup> The stiff-spring approximation relating  $F$  to the PMF ( $\Phi$ ) (eq 2)<sup>5–7</sup> was satisfied with  $k = 40 \text{ kcal mol}^{-1} \text{ \AA}^{-2}$ . The PMF along the unbinding reaction coordinate was reconstructed from the SMD trajectories described above using Jarzynski's equality (eq 3),<sup>6–8</sup> which relates the Helmholtz free energy ( $F$ ) to  $W$  and  $\beta = (k_B T)^{-1}$ . The cumulant expansion approach up to second order (eq 4)<sup>6–8</sup> was used to reconstruct the PMF.

$$W_{[x(t)]} = \int_0^{x(t)} F_{\text{ex}}(t) \, dx(t) \quad (1)$$

$$F(\lambda) \approx \Phi(\lambda) \quad (2)$$

where  $\lambda$  is external parameter defined in such a way that  $\lambda$  is correlated with the reaction coordinate of the studied system

$$e^{-\beta \Delta F} = \langle e^{-\beta W} \rangle \quad (3)$$

$$\Delta F = \langle W \rangle - \frac{\sigma_W^2}{2k_B T} \quad (4)$$

where  $\sigma_W^2 = \langle W^2 \rangle - \langle W \rangle^2$  and  $k_B T = 0.6186 \text{ kcal/mol}$ .

## RESULTS

**Calibration of the Pulling Velocity and Force Constant.** The first set of experiments were carried out on the last frame of the *NVT* trajectory of each ligand and were devoted to the optimization of the velocity while keeping the force constant fixed. In order to accomplish these trials, the reaction coordinate was tentatively defined as the distance between the ligand centroid and the C $\alpha$  atom of V899 buried in the ATP binding site. For this purpose, the force constant  $k$  was fixed at  $15 \text{ kcal mol}^{-1} \text{ \AA}^{-2}$  while different velocities of 0.0001, 0.0002, 0.00025, 0.0005, 0.001, and 0.01 Å/ps were studied. At the end of each experiment, the end-to-end distance of each frame was plotted versus the actual reaction coordinate. As shown in Figures 4 and 5, even for the slowest simulation performed with  $v = 0.0001 \text{ \AA/ps}$  for a 1 Å reaction coordinate displacement, the force constant seemed to be too loose, preventing the stiff-spring approximation from being satisfied, in particular for the more tightly bound ligand sorafenib (Figure 5). Further reduction of the constant velocity was not tried, as the estimated simulation time would have been prohibitive. For example, a 1 Å reaction coordinate displacement performed with  $v = 0.0001 \text{ \AA/ps}$  and  $k = 15 \text{ kcal mol}^{-1} \text{ \AA}^{-2}$  lasted more than 23 h (64 CPU processors, Cineca Eurora). As expected, experiments performed with higher pulling velocities ( $v = 0.001$  and 0.01 Å/ps) confirmed that the systems were not able to follow the guiding potential and that the stiff-spring approximation was not satisfied (the data are reported in Figures S1 and S2 in the Supporting Information).

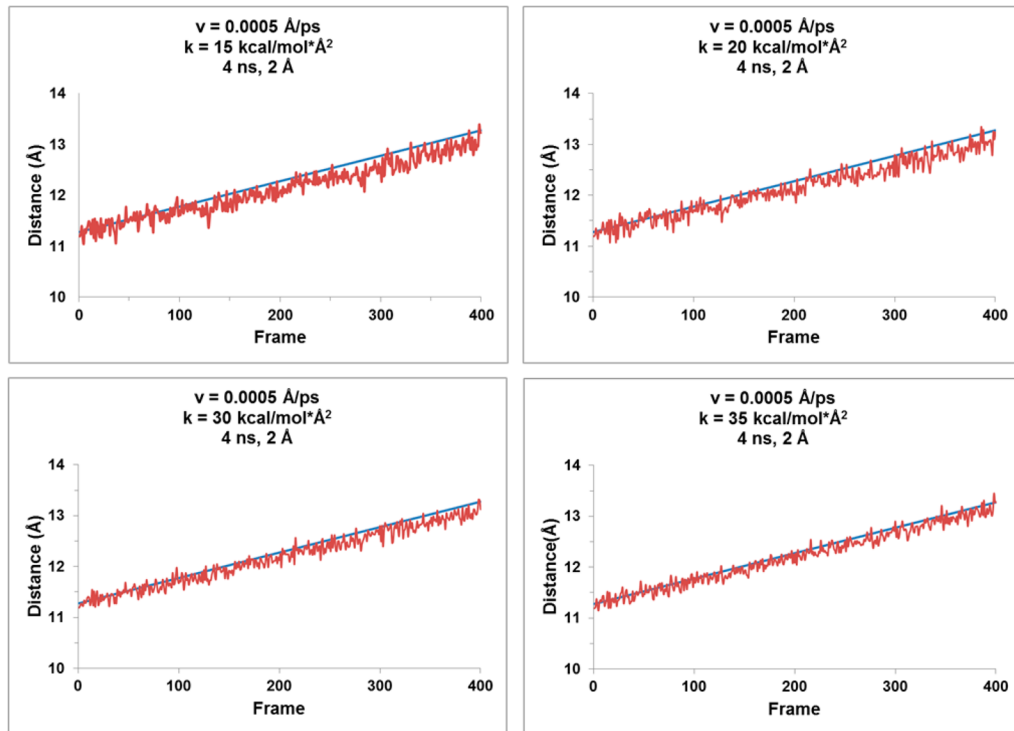


**Figure 6.** Plots of the end-to-end distance (red line) and the constrained distance (blue line) (Y axis) measured in each frame (X axis) in simulations of the VEGFR2/SUN complex performed with  $v = 0.0005 \text{ \AA}/\text{ps}$  and  $k = 15, 20, 30$ , and  $35 \text{ kcal mol}^{-1} \text{ \AA}$ . The average values of the absolute difference between the theoretical and real distances measured in the simulations performed with  $k = 30$  and  $35 \text{ kcal mol}^{-1} \text{ \AA}$  are comparable (0.11 vs 0.098).

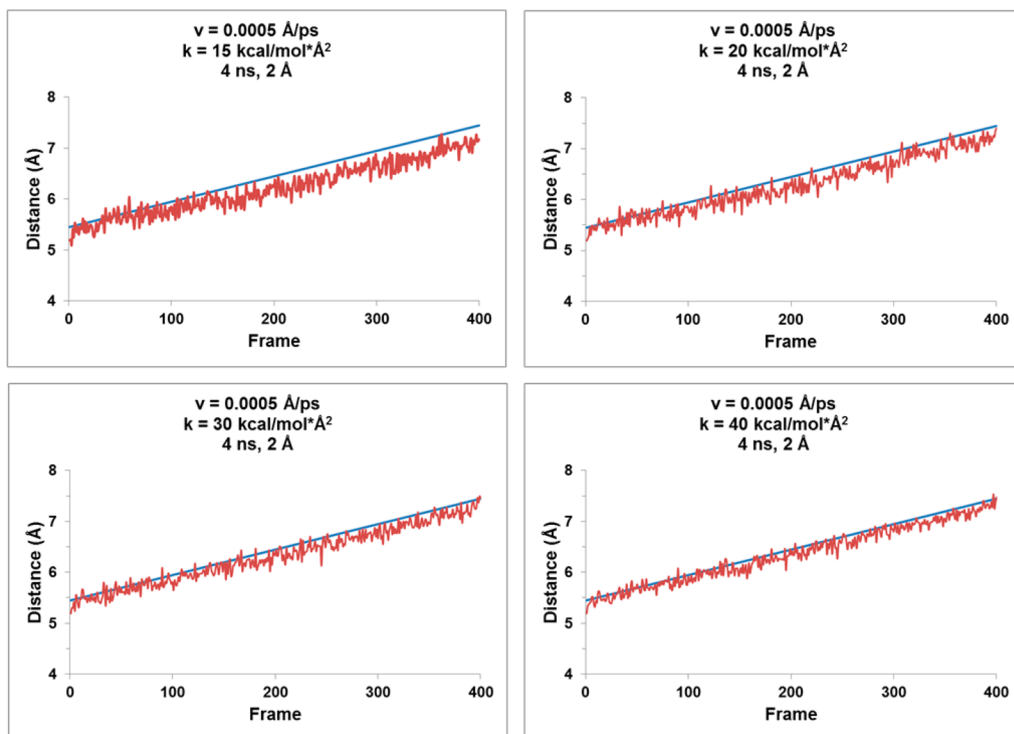


**Figure 7.** Plots of the end-to-end distance (red line) and the constrained distance (blue line) (Y axis) measured in each frame (X axis) in simulations of the VEGFR2/SOR complex performed with  $v = 0.0005 \text{ \AA}/\text{ps}$  and  $k = 15, 20, 30$ , and  $40 \text{ kcal mol}^{-1} \text{ \AA}^{-2}$ . In light of these results, the parameter values  $v = 0.0005 \text{ \AA}/\text{ps}$  and  $k = 40 \text{ kcal mol}^{-1} \text{ \AA}^{-2}$  were used for subsequent studies, as they represent the best trade-off between accuracy and calculation time.

In light of these experiments,  $v$  was fixed at  $0.0005 \text{ \AA}/\text{ps}$  while  $k$  was set at  $15, 20, 25, 30, 35$ , and  $40 \text{ kcal mol}^{-1} \text{ \AA}^{-2}$  (4

ns simulation, 400 frames sampled per run). The simulations performed for the VEGFR2/SUN complex (Figure 6) showed

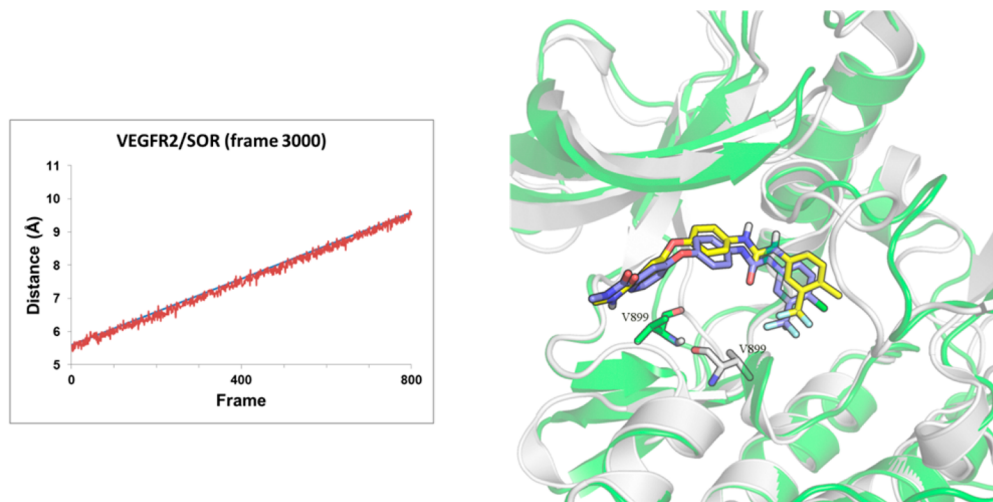


**Figure 8.** SMD simulation of VEGFR2/SOR performed by setting the reaction coordinate as the distance between the  $\text{C}\alpha$  atom of V899 and the centroid of sorafenib. (left) Plot of the end-to-end distance (blue line) and the actual value (red line) of the reaction coordinate. (right) Overlay of the VEGFR2/SOR X-ray structure (protein ribbon gray, ligand C atoms blue) with respect to the last frame sampled after simulation for 8 ns (protein ribbon green, ligand C atoms yellow).

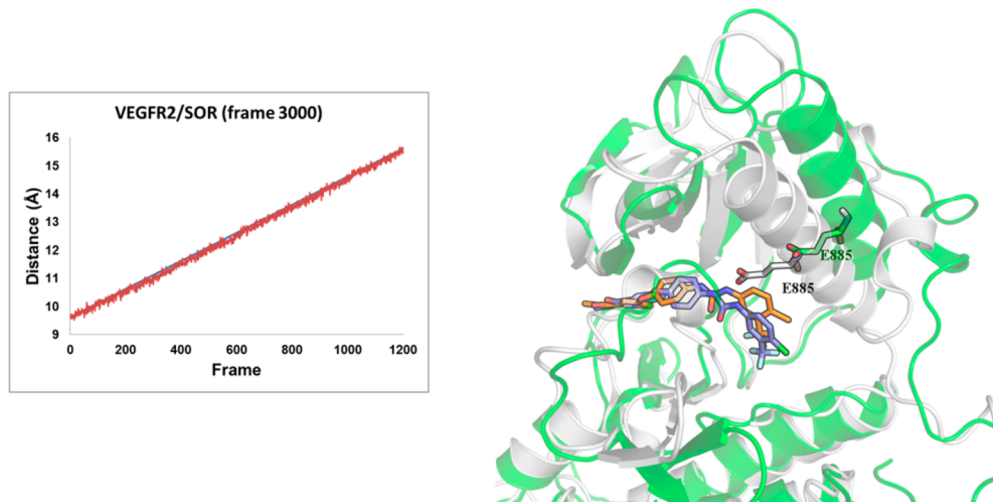


**Figure 9.** SMD simulation of VEGFR2/SOR performed by setting the reaction coordinate as the distance between the  $\text{C}\alpha$  atom of E885 and the centroid of sorafenib. (left) Plot of the end-to-end distance (blue line) and the actual value (red line) of the reaction coordinate. (right) Overlay of the VEGFR2/SOR X-ray structure (protein ribbon gray, ligand C atoms blue) with respect to the last frame sampled after simulation for 12 ns (protein ribbon green, ligand C atoms orange).

that the stiff-spring approximation was satisfied when  $k$  was increased to  $30 \text{ kcal mol}^{-1} \text{ Å}^{-2}$ . On the contrary, the more tightly bound VEGFR2/SOR complex (Figure 7) required a stiffer force constant, and the stiff-spring approximation was fulfilled only when  $k = 40 \text{ kcal mol}^{-1} \text{ Å}^{-2}$ . Further increasing the force constant ( $k = 45 \text{ kcal mol}^{-1} \text{ Å}^{-2}$ ; see the Supporting Information) provided very similar results, suggesting that  $k = 40 \text{ kcal mol}^{-1} \text{ Å}^{-2}$  is the minimum value required in order to satisfy the stiff-spring approximation. This simulation lasted for 12 h/processor (64 processors in total). No significant changes in the conformation of the enzyme were observed during these calibration experiments.

**Selection of the Unbinding Reaction Coordinate.** Subsequent SMD simulations were devoted to the identification of the most appropriate unbinding reaction coordinate, whose selection was based on visual inspection of the crystal complexes.

In the first experiment, the reaction coordinate was defined as the distance between the ligand center of mass and the  $\text{C}\alpha$  atom of V899, which lies approximately in the middle of the ligand binding site. SMD simulations of equilibrated VEGFR2/SOR frame 3000 were performed by moving along the reaction coordinate between 0 and 4 Å in steps of 2 Å with  $v = 0.0005 \text{ Å}/\text{ps}$  and  $k = 40 \text{ kcal mol}^{-1} \text{ Å}^{-2}$ . At the end of the 8 ns long simulation (800 frames sampled), even though the stiff-spring approximation was fairly well satisfied (Figure 8, left), a remarkable change was observed in the conformation of the loop hosting V899, higher than the 2 Å crystal structure resolution. On the contrary, the ligand conformation and orientation in the binding site were very similar to those in the crystal structures (Figure 8, right).

In light of these results, the reaction coordinate was defined as the distance between the center of mass of the ligand and the  $\text{C}\alpha$  atom of E885 belonging to the  $\alpha\text{C}$ -helix. This residue is involved in a salt-bridge interaction with K868 and lies

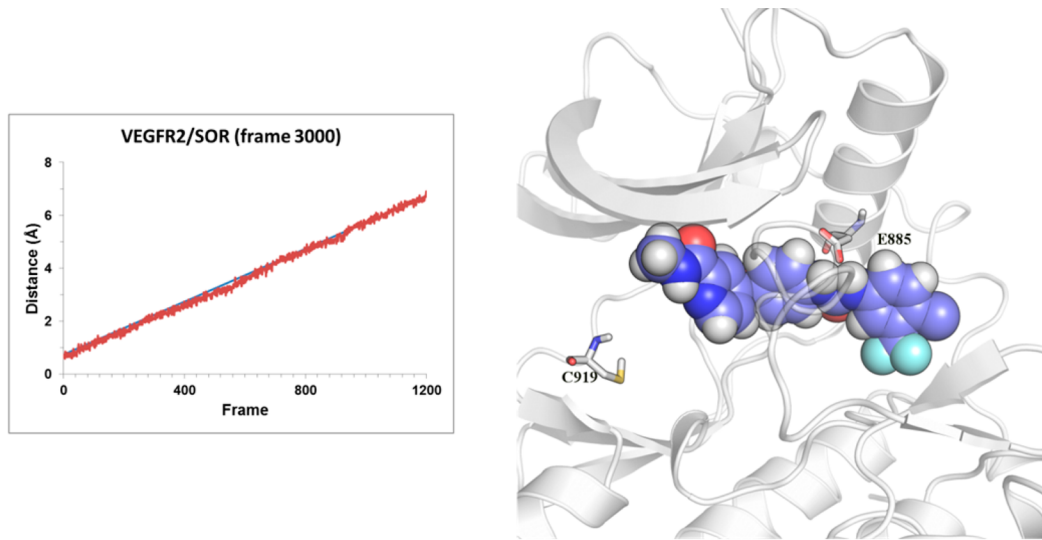


**Figure 10.** SMD simulation of VEGFR2/SOR performed by setting the reaction coordinate as the distance between the centroid of the sorafenib binding site and the sorafenib center of mass. (left) Plot of the end-to-end distance (blue line) and the actual value (red line) of the reaction coordinate. (right) The last frame sampled after simulation for 12 ns (6 Å reaction coordinate displacement). This picture highlights that sorafenib leaves the binding site by moving toward the JM domain rather than the entrance of the ATP pocket, marked by the C919 hinge residue.

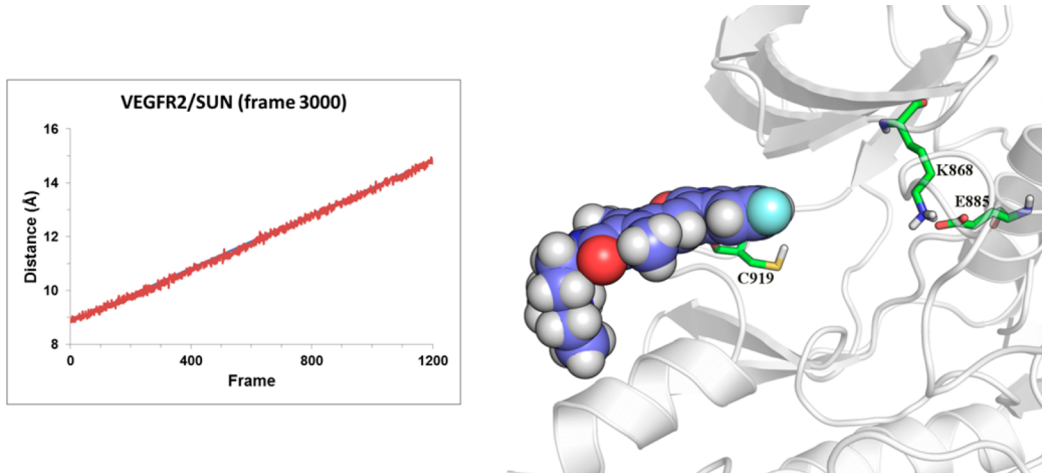


**Figure 11.** SMD simulation of the VEGFR2/SUN performed by setting the reaction coordinate as the distance between the centroid of the sorafenib binding site and the sunitinib center of mass. (left) Plot of the end-to-end distance (blue line) and the actual value (red line) of the reaction coordinate. (right) The last frame sampled after simulation for 12 ns (6 Å reaction coordinate displacement). This picture highlights that in contrast to sorafenib, sunitinib leaves the binding site by moving toward the entrance of the ATP pocket, marked by the C919 hinge residue.

approximately in the middle of the inhibitor binding sites. Frames no. 3000 of both the systems under study were then simulated by moving along the new reaction coordinate between 0 and 6 Å in steps of 2 Å. The pulling velocity and the force constant were set as in the previous experiments ( $v = 0.0005 \text{ Å}/\text{ps}$  and  $k = 40 \text{ kcal mol}^{-1} \text{ Å}^{-2}$ ). In Figure 9 are reported the results of the simulations performed for the VEGFR2/SOR complex. As shown, the stiff-spring approximation was well satisfied (Figure 9, left). However, visual inspection of the frames sampled between 4 and 6 Å highlighted a remarkable movement of the  $\alpha$ C-helix while the loop hosting V899 fluctuated within the crystal structure resolution (Figure 9, right). At the same time, the ligand did not significantly change its orientation and conformation with respect to those observed in the crystal structure (Figure 9, right). Similar results were obtained for the VEGFR2/SUN complex (see Figure S3 in the Supporting Information). Hence,

these data suggest that the  $\alpha$ C-helix displacement is most likely an artifact of the SMD simulations.

Further experiments using alternative reaction coordinate definitions were performed, as detailed in Figures S4–S8 in the Supporting Information. However, many of them led to even more dramatic changes in the enzyme spatial arrangement. Only when the reaction coordinate was defined as the distance between the ligand center of mass and the centroid of the sorafenib binding site was sorafenib able to find a way out of the VEGFR2 binding site without disrupting the enzyme conformation. As shown in the left panel of Figure 10, the stiff-spring approximation was well satisfied. Besides, in the frame sampled at the end of the 12 ns long trajectory (Figure 10, right) sorafenib escaped from the enzyme binding site by moving toward the JM domain rather than the ATP binding site entrance leading to a change in the spatial orientation of the  $\alpha$ C-helix.

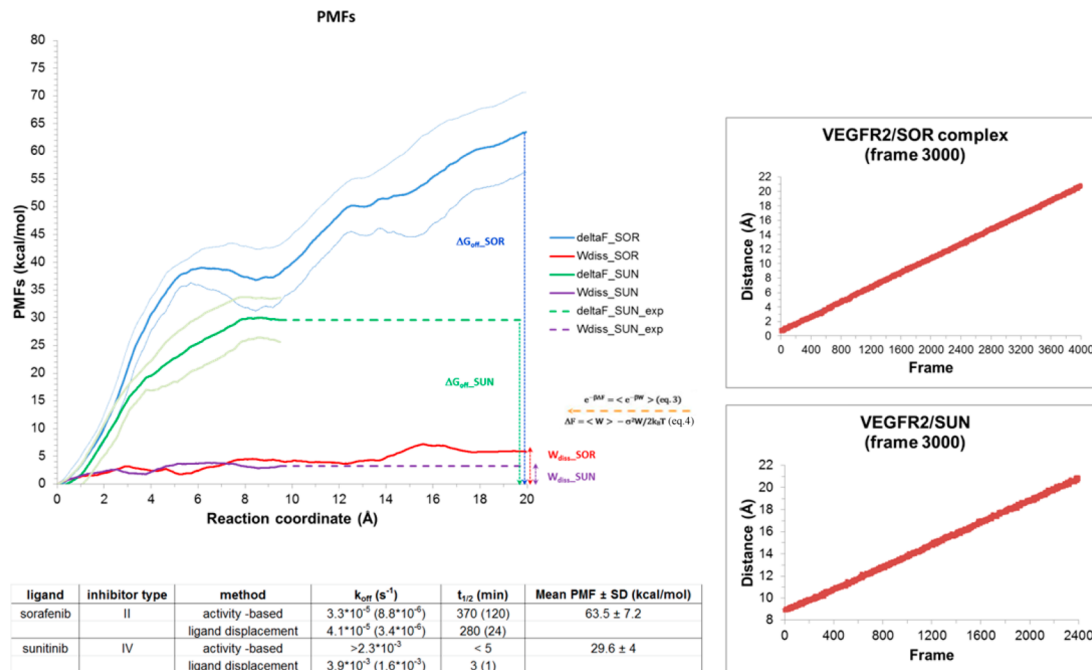


**Figure 12.** (left) PMF profiles of sunitinib and sorafenib. (right) Comparisons of end-to-end and constrained distances from representative frames for the two ligands.

The simulation performed with the VEGFR2/SUN complex under the same conditions showed that the stiff-spring approximation was well satisfied (Figure 11, left). In contrast to the VEGFR2/SOR complex, this ligand left the enzyme cavity from the ATP binding site entrance (Figure 11, right) with no remarkable change in the enzyme conformation.

Following these encouraging results, the reaction coordinate of sorafenib was explored up to a total displacement of 20 Å (40 ns long simulations), while that of sunitinib was sampled up to a total displacement of 12 Å, at which point the ligand lies outside the binding site.

**PMFs along the Unbinding Reaction Coordinates.** The comparison of end-to-end and constrained distances shown in Figure 12 (right) proves that the stiff-spring approximation was satisfied when a low pulling velocity of 0.0005 Å/ps and a force constant of 40 kcal mol<sup>-1</sup> Å<sup>-2</sup> was used. By application of Jarzynski's equality (eq 3) and the cumulative expansion up to second order (eq 4), the PMF of each ligand was reconstructed (average of each simulation work), and the results are plotted versus the reaction coordinate in Figure 12 (left).

The analysis in Figure 12 (left) reveals that the PMF of sorafenib (mean  $\pm$  SD = 63.5  $\pm$  7.2 kcal/mol) is higher than that of sunitinib (29.6  $\pm$  4 kcal/mol). This result is qualitatively in agreement with the experimental  $k_{\text{off}}$  and residence time values of these derivatives reported in the inset table at the bottom of the figure.<sup>17</sup> Furthermore, the energy basin of sorafenib is narrower than that of sunitinib, suggesting that sunitinib can dissociate from VEGFR2 following different pathways. The dissipated work  $\Delta W_{\text{diss}}$  shown in Figure 12 refers to the strength of friction representing the irreversible work dissipated as a result of nonequilibrium conditions. The value of  $\Delta W_{\text{diss}}$  for sorafenib and sunitinib (2.6 kcal/mol) is much lower than the difference in their calculated PMFs ( $\Delta F_{\text{SOR}} - \Delta F_{\text{SUN}} = 33.9$  kcal/mol), supporting the reliability of the difference observed for the calculated PMFs in our SMD simulations.

**Analysis of the Dissociation Pathways.** Figure 13 shows a plot of the force profile and selected snapshots taken from the simulation of sorafenib exhibiting the lowest work value (frame 3000). Snapshot 1 was taken at the beginning of the simulation and shows that the sorafenib urea moiety forms a hydrogen-bonding (HB) interaction with D1046 (DFG-out motif) and two charge-reinforced HB interactions with E885, which makes a salt bridge with K868. This lysine in turn interacts with the carbonyl backbone of D1046. Hence, the ligand is tightly bound to VEGFR2 by this network of HB interactions that bridges residues in the N lobe (K868, E885) to those in the C lobe (D1046 in the activation loop) and narrows the binding site. Hence, sorafenib appears to be trapped in a gorge of the binding pocket. Furthermore, the *m*-trifluoromethyl-*p*-chlorophenyl ring forms a hydrophobic interaction with L889 at the end of the  $\alpha$ C-helix and is projected into a widely open solvent-exposed region of the binding site. Finally, the pyridyl fragment forms a HB interaction with the hinge residue C919. Between 0 and 2 Å of reaction coordinate displacement, there is an increase in the force value, which is due to the disruption of the direct HB interactions established by the ligand pyridine fragment and its acetylamide NH with the NH backbone of the hinge amino acid C919. The breakage of such interactions is assisted by a solvent water molecule (snapshot 2). Between 2 and 4 Å of reaction coordinate displacement the HB interaction involving the carbonyl group of the ligand urea and the NH backbone of D1046 is lost (snapshot 3). Besides, only one HB interaction is made by the ligand urea with E885. At the same time the *m*-trifluoromethyl-*p*-chlorophenyl fragment approaches some hydrophobic residues in the  $\alpha$ C-helix (I888, I892) while the core ligand phenyl ring moves close to L889. As a result, the orientation of the  $\alpha$ C-helix changes in order to facilitate ligand exit toward the JM domain (snapshot 4). Between 4 and 6 Å of reaction coordinate displacement, one of the ligand urea NH moieties is still involved in a HB interaction with E885, delaying the ligand exit (snapshot 5). Beyond 6 Å of

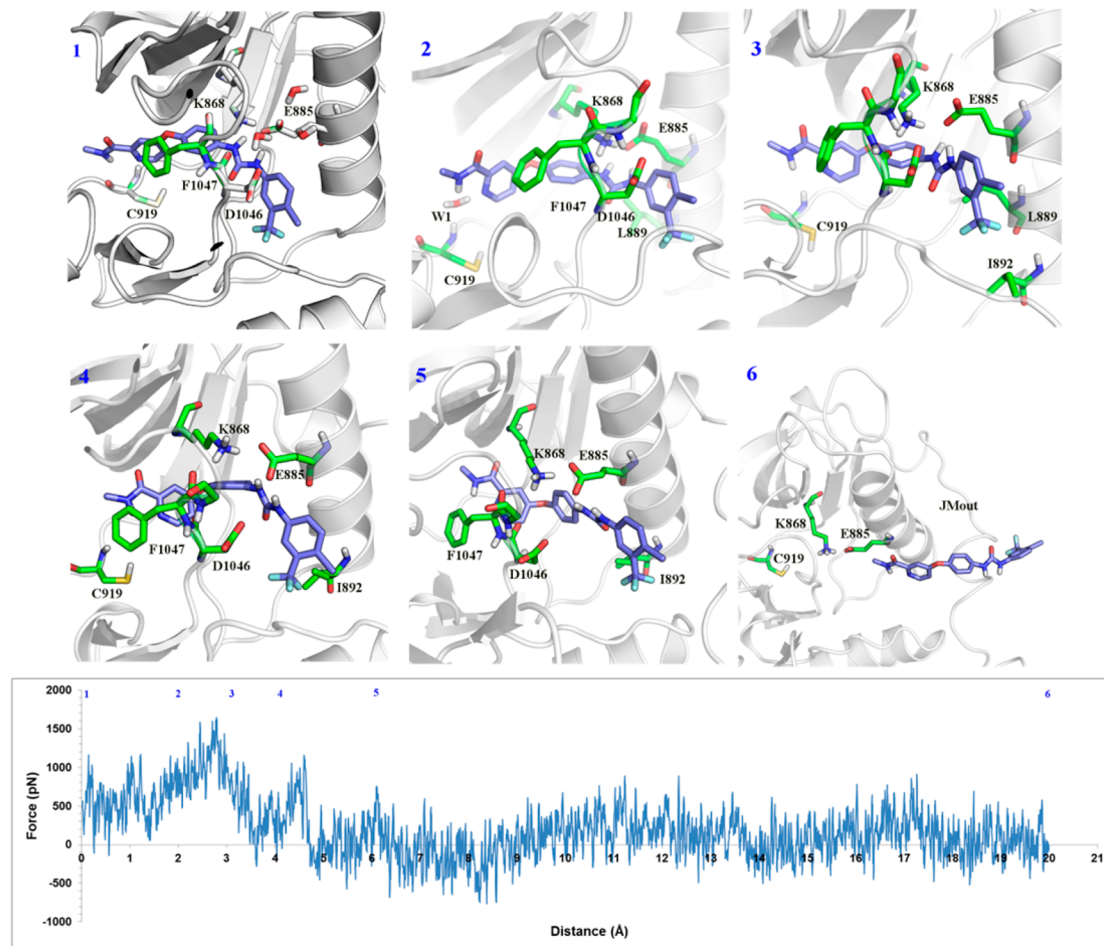


**Figure 13.** (top) Representative frames from the simulation of the VEGFR2/SOR complex exhibiting the lowest work value (frame 3000). (bottom) Force profile of sorafenib (frame 3000) as a function of the reaction coordinate.

reaction coordinate displacement, the force profile is relatively flat, and the ligand lies outside the ATP binding site but is still close to the JM domain (snapshot 6).

The force profile of the sunitinib frame exhibiting the lowest work profile, shown in Figure 14 (bottom), suggests that in contrast to sorafenib, the sunitinib unbinding pathway does not require the disruption of any strong interactions. At the beginning of the simulation (snapshot 1), sunitinib forms two HB interactions with the hinge residue C919 and with E917. Besides, the aromatic ring of the ligand forms hydrophobic contacts with F1047 (DFG-out motif) and L840 in the P loop. Between 0 and 2 Å of reaction coordinate displacement, the hydrogen bond with E917 is broken while that with the hinge residue becomes looser and acts as a pivot, delaying the ligand exit (snapshot 2). At the same time, the interactions with F1047 become less strong. Between 2 and 4 Å of reaction coordinate displacement, the hinge HB interaction is weaker (snapshot 3), and the ligand is almost entirely exposed to the solvent. Between 4 and 12 Å of reaction coordinate displacement, the ligand has left the ATP binding site. However, it still makes contacts with some solvent-exposed amino acids (E934, K931, S930, and T926) in an  $\alpha$ -helix (snapshot 4).

## ■ DISCUSSION

SMD is a theoretically well-established methodology that has been extensively applied to the study of mechanical unfolding

of biomolecules, transportation of ions and organic compounds through membrane channels, and unbinding pathways of ligands from their receptors. Recently SMD has been also been coupled to docking experiments in order to improve the efficacy of a virtual screening exercise and to rationalize structure–activity data.<sup>2–9</sup> The expansion of its traditional domain of applicability to drug design case studies has been possible because of the availability of powerful computational infrastructures (GPUs) and software engineering. Herein we set up SMD experiments within Amber to model the unbinding pathways of sorafenib and sunitinib from VEGFR2. This is a challenging case study because of the high flexibility of the target (e.g., DGF motif,  $\alpha$ C-helix), its huge size (68k atoms including the solvent box), and the properties of the binding site, which is wide open and solvent-exposed.

The most critical aspect of the simulations performed is represented by the selection of the unbinding reaction coordinate. In principle, the use of random approaches such as RAMD<sup>21</sup> would have facilitated the identification of suitable ligand exit paths. Unfortunately, this automated procedure has not been implemented in the Amber software. Hence, our selection was based on visual inspection of the crystal structures. Subsequently, potential reaction coordinates were explored following a time-consuming and resource-intensive trial and error approach. As a result, the reaction coordinate defined as the distance between the sorafenib binding site and the ligand center of mass proved to be the most appropriate

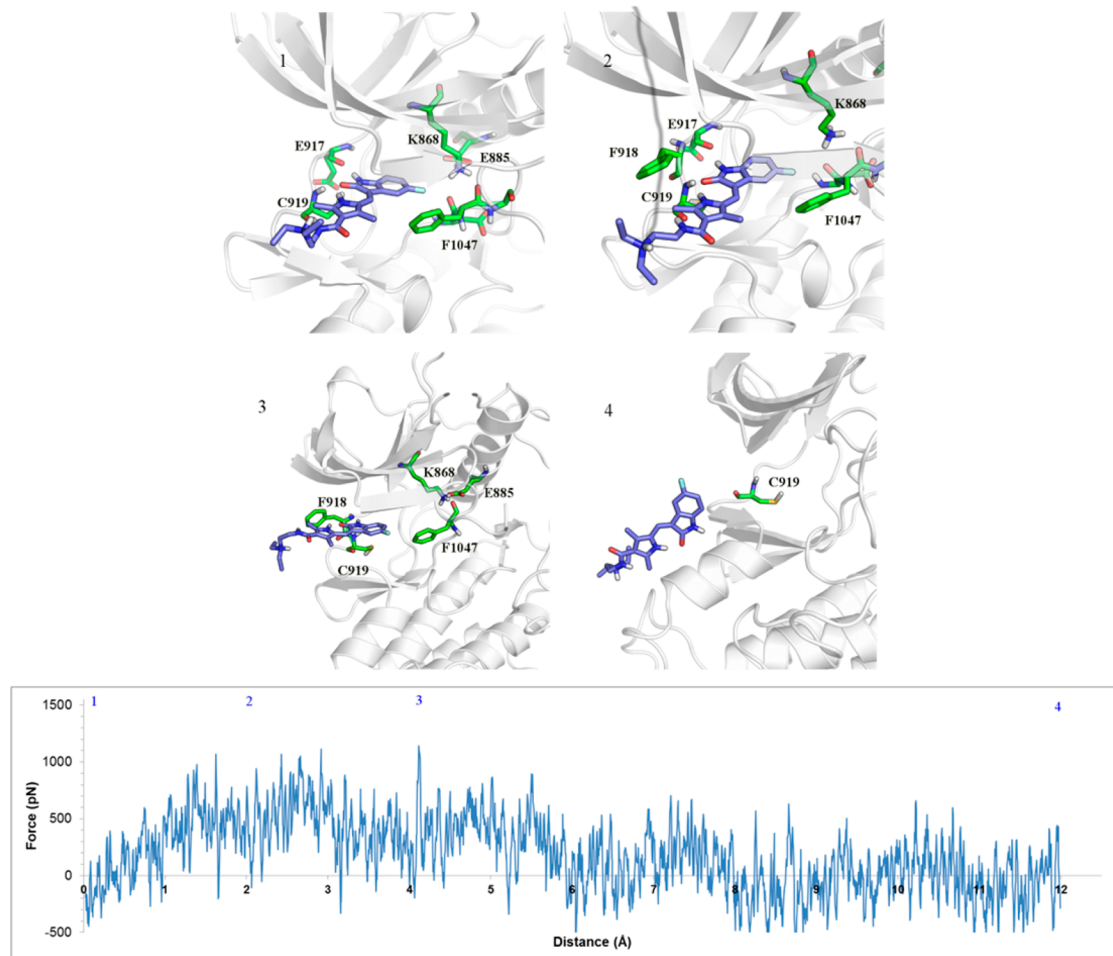


**Figure 14.** (top) Representative frames from the simulation of the VEGFR2/SUN complex exhibiting the lowest work value (frame 3000). (bottom) Force profile of sunitinib as a function of the reaction coordinate.

among those analyzed, as it did not lead to a dramatic change in the kinase conformation. Despite this biased selection, the SMD simulations of sorafenib and sunitinib were performed without forcing them to follow a predefined direction, and they found their own ways to escape from the enzyme pocket. However, it cannot be ruled out that these ligands could potentially follow other unbinding pathways. To prove that, other techniques such as metadynamics simulations could be used to model ligand unbinding and enzyme conformational changes simultaneously.<sup>22</sup> Besides, site-directed mutagenesis experiments of amino acids involved in ligand unbinding, in particular those lying at the end of the  $\alpha$ C-helix, could be performed in order validate these simulations.

Subsequent to the identification of an appropriate reaction coordinate, the SMD simulations required the calibration of the pulling force and the force constant, as they both strictly depend on the system under study. The selection of their optimal combination,  $v = 0.0005 \text{ Å}/\text{ps}$  and  $k = 40 \text{ kcal mol}^{-1} \text{ Å}^{-2}$ , was the result of a trade-off between fulfillment of the stiff-spring approximation and the power of the computational infrastructure used to accomplish these calculations. Lower pulling velocities could not be utilized because of IT infrastructure constraints. The force constant used is quite stiff ( $k = 40 \text{ kcal mol}^{-1} \text{ Å}^{-2}$ ), but it represents the minimum value required by the sorafenib simulations to satisfy the stiff-

spring approximation. This value likely reflects its tight binding to this enzyme (subnanomolar pIC<sub>50</sub> value).<sup>14</sup>

Furthermore, SMD simulations had to be repeated on a few frames (five for sorafenib, four for sunitinib) to achieve statistical robustness. This in turn required the availability of a powerful computational infrastructure.

The results of the SMD simulations performed reveal that sunitinib leaves the ATP binding site through the cavity entrance. The forces involved are weak, and there are no significant changes in the enzyme conformation upon ligand unbinding. The main ligand–enzyme interaction is represented by the hydrogen bond involving the hinge residue, which acts as pivot that delays the ligand exit. On the contrary, sorafenib leaves the ATP binding site opposite to the cavity entrance and moves toward the JM domain. The HB interaction established with the hinge residue is lost in the first 2 Å of displacement along the reaction coordinate. The breakage of such an interaction is assisted by a water molecule that bridges the ligand to this amino acid. Besides, the ligand urea moiety forms hydrogen bonds with E885 and D1046 and lies in a narrow region of the binding site where a network of protein–ligand HB interactions is established. Hence, it is likely that the presence of this tight network of HB interactions and the limited size of this subpocket delay the ligand exit and force the  $\alpha$ C-helix to change its spatial orientation. Besides, the ligand phenyl ring decorated with hydrophobic electron-withdrawing

substituents establishes lipophilic contact with some hydrophobic amino acids in the  $\alpha$ C-helix and moves close to them during unbinding. After 20 Å of reaction coordinate displacement, sorafenib has left the ATP binding site but lies near the JM domain. In light of that, further exploration of the reaction coordinate is required in order to have the ligand fully solvated.

Finally, the reconstructed PMF of sorafenib is higher than that of sunitinib. This result is qualitatively in agreement with the experimental  $k_{\text{off}}$  and residence time values of these derivatives.<sup>17</sup> At the same time, their values for the dissipated work are comparable to each other and lower than the difference of their PMFs. In light of these results, the SMD protocol developed here appears to be very promising, as it provides valuable drug design suggestions and qualitative energy estimation in line with the kinetic parameters. Hence, more ligands could be modeled to further increase its robustness.

## CONCLUSIONS

VEGFR2 is a clinically validated target in the oncology field. Medicinal chemistry efforts aimed at finding potent inhibitors of this receptor tyrosine kinase led to the identification of sunitinib and sorafenib, both of which on the market to treat renal cell carcinoma. While sunitinib quickly dissociates from VEGFR2, sorafenib exhibits quite a long residence time at this enzyme, which might impact its duration of action *in vivo*.

Herein a detailed atomistic description of the unbinding process of sorafenib and sunitinib was unraveled by using SMD simulations. While sunitinib exits the ATP binding site from the cavity entrance without a rupture point, sorafenib moves opposite to the ATP binding site entrance and approaches the JM domain, causing a change in the orientation of the  $\alpha$ C-helix. Its unbinding pathway is delayed by the involvement of its urea moiety in a strong hydrogen-bonding network with D1046 (DFG-out motif) as well as E885 in the  $\alpha$ C-helix. Besides, this unbinding process is slowed by the formation of hydrophobic interactions of the ligand pendant phenyl ring with some  $\alpha$ C-helix residues. In addition to this valuable structural information, the calculated values of  $\Delta G_{\text{off}}$  for both these ligands clearly reflect their distinct off-rates on a qualitative level, suggesting that this protocol could be tried on other VEGFR2 ligands to assess its robustness and then used to rank structural analogues of these derivatives.

Even though the theoretical background of this methodology is relatively simple, there are critical aspects that have to be addressed on a case-by-case base. First of all, the identification of the unbinding reaction coordinate might not be straightforward. The use of a “trial and error” approach, even if inspired by knowledge of the enzyme–ligand structure, proved to be time-consuming and computer-resource-demanding. Besides, the calibration of the pulling velocity and the force constant was computationally intensive, and the selection of the most appropriate combination of these parameters was basically a trade-off between the fulfillment of the stiff-spring approximation and the constraints of available computer resources. Finally, the SMD simulations had to be repeated on some frames to increase the robustness of the results achieved, which again implies the need for a powerful computational infrastructure.

Despite these critical aspects and the significant amount of computer resources required, the application of SMD to study the unbinding pathways of these ligands proved to be very informative and valuable for drug design purposes. Hence, it is

likely that SMD as well as other enhanced sampling methods will become more popular in the computational chemistry community in the years to come.

## ASSOCIATED CONTENT

### Supporting Information

Details related to further experiments for pulling velocity and force constant calibrations as well as determination of the unbinding reaction coordinate. This material is available free of charge via the Internet at <http://pubs.acs.org>.

## AUTHOR INFORMATION

### Corresponding Author

\*E-mail: Gabriele.costantino@unipr.it. Phone: +39 0521 905055.

### Notes

The authors declare no competing financial interest.

## ACKNOWLEDGMENTS

A.M.C. thanks Dr. Maurizio Delcanale (Chiesi Farmaceutici S.p.A) for supporting her Ph.D study. G.C. and A.M.C. acknowledge the CINECA Consortium for computational support and resources (Grants IsC11\_VEG-IN, IsC13\_VEG-IN-2, and IsC16\_VEG-IN-3) and Prof. Andrea Cavalli and Dr. Agostino Bruno for helpful discussions.

## ABBREVIATIONS

VEGFR2, vascular endothelium growth factor receptor 2; RAMD, random accelerated molecular dynamics; SMD, steered molecular dynamics; RMSD, root-mean-square deviation; PMF, potential of mean force.

## REFERENCES

- (1) Copeland, R. A.; Pomialiano, D. L.; Meek, T. D. Drug Target Residence Time and Its Implication in Lead Optimization. *Nat. Rev. Drug Discovery* **2006**, *5*, 730–739.
- (2) Colizzi, F.; Perozzo, R.; Scapozza, L.; Recanatini, M.; Cavalli, A. Single-Molecule Pulling Simulations Can Discern Active from Inactive Enzyme Inhibitors. *J. Am. Chem. Soc.* **2010**, *132*, 7361–7371.
- (3) Suresh Patel, J.; Bertotti, A.; Ronisvalle, S.; Rocchia, W.; Cavalli, C. Steered Molecular Dynamics Simulations for Studying Protein–Ligand Interaction in Cyclin-Dependent Kinase 5. *J. Chem. Inf. Model.* **2014**, *54*, 470–480.
- (4) Kalyaanamoorthy, S.; Chen, Y.-P. P. A Steered Molecular Dynamics Mediated Hit Discovery for Histone Deacetylases. *Phys. Chem. Chem. Phys.* **2014**, *16*, 3777–3791.
- (5) Zhang, J.-L.; Zheng, Q.-C.; Li, Z.-Q.; Zhang, H.-X. How Does (E)-2-(Acetamidomethylene)succinate Bind to Its Hydrolase? From the Binding Process to the Final Result. *PLoS One* **2013**, *8*, No. e53811.
- (6) Shen, Z.; Cheng, F.; Xu, Y.; Fu, J.; Xiao, W.; Shen, J.; Liu, G.; Li, W.; Tang, Y. Investigation of Indazole Unbinding Pathways in CYP2E1 by Molecular Dynamics Simulations. *PLoS One* **2012**, *7*, No. e33500.
- (7) Miño, G.; Baez, M.; Gutierrez, G. Effect of Mutation at the Interface of Trp-repressor Dimeric Protein: A Steered Molecular Dynamics Simulation. *Eur. Biophys. J.* **2013**, *42*, 683–690.
- (8) Mai, B. K.; Li, M. S. Neuraminidase Inhibitor R-125489—A Promising Drug for Treating Influenza Virus: Steered Molecular Dynamics Approach. *Biochem. Biophys. Res. Commun.* **2011**, *410*, 688–691.
- (9) Capelli, A. M.; Bruno, A.; Entrena Guadix, A.; Costantino, G. Unbinding Pathways from Glucocorticoid Receptor Shed Light on Reduced Sensitivity of Glucocorticoid Ligands to a Naturally

Occurring, Clinically Relevant, Mutant Receptor. *J. Med. Chem.* **2013**, *56*, 7003–7014.

(10) Jarzynski, C. Nonequilibrium Equality for Free Energy Differences. *Phys. Rev. Lett.* **1997**, *78*, 2690–2693.

(11) Park, S.; Khalili-Araghi, F.; Tajkhorshid, E.; Schulten, K. Free Energy Calculation from Steered Molecular Dynamics Simulations Using Jarzynski's Equality. *J. Chem. Phys.* **2003**, *119*, 3559–3566.

(12) Park, S.; Schulten, K. Calculating Potentials of Mean Force from Steered Molecular Dynamics Simulations. *J. Chem. Phys.* **2004**, *120*, 5946–5961.

(13) Rini, B. I.; Escudier, B.; Tomczak, P.; Kaprin, A.; Szczylik, C.; Hutson, T. E.; Michaelson, D.; Gorbunova, V. A.; Gore, M. E.; Rusakov, I. G.; Negrier, S.; Ou, Y.-C.; Castellano, D.; Yeong Lim, H.; Uemura, H.; Tarazi, J.; Cella, D.; Chen, C.; Rosbrook, B.; Kim, S.; Motzer, R. J. Comparative Effectiveness of Axitinib versus Sorafenib in Advanced Renal Cell Carcinoma (AXIS): A Randomised Phase 3 Trial. *Lancet* **2011**, *378*, 1931–1939.

(14) McTigue, M.; Murray, B. W.; Chen, J. H.; Deng, Y.-L.; Solowiej, J.; Kania, R. S. Molecular Conformations, Interactions, and Properties Associated with Drug Efficiency and Clinical Performance among VEGFR TK Inhibitors. *Proc. Natl. Acad. Sci. U.S.A.* **2012**, *109*, 18281–18289.

(15) Muñoz, C.; Adasme, F.; Alzate-Morales, J. H.; Vergara-Jaque, A.; Kniss, T.; Caballero, J. Study of Differences in the VEGFR2 Inhibitory Activities between Semaxanib and SU5205 using 3D-QSAR, Docking, and Molecular Dynamics Simulations. *J. Mol. Graphics. Modell.* **2012**, *32*, 39–48.

(16) Caballero, J.; Muñoz, C.; Alzate-Morales, J. H.; Cunha, S.; Gano, L.; Bergmann, R.; Steinbach, J.; Kniss, T. Synthesis, in Silico, in Vitro, and in Vivo Investigation of 5-[<sup>11</sup>C]methoxy-Substituted Sunitinib, a Tyrosine Kinase Inhibitor of VEGFR-2. *Eur. J. Med. Chem.* **2012**, *58*, 272–280.

(17) Iwata, H.; Imamura, S.; Hori, A.; Hixon, M. S.; Kimura, H.; Miki, H. Biochemical Characterization of a Novel Type-II VEGFR2 Kinase Inhibitor: Comparison of Binding to Non-phosphorylated and Phosphorylated VEGFR2. *Bioorg. Med. Chem.* **2011**, *19*, 5342–5351.

(18) Maestro, version 9.1; Schrödinger, LLC: New York, 2009; <http://www.schrodinger.com/>.

(19) The AMBER Molecular Dynamics Package; <http://ambermd.org/>.

(20) VMD, version 1.8.7 (Aug 1, 2009): Humphrey, W.; Dalke, A.; Schulten, K. VMD—Visual Molecular Dynamics. *J. Mol. Graphics* **1996**, *14*, 33–38 ; <http://www.ks.uiuc.edu/Research/vmd/>.

(21) Ludemann, S. K.; Lounnas, V.; Wade, R. C. How Do Substrates Enter and Products Exit the Buried Active Site of Cytochrome P450cam? 1. Random Expulsion Molecular Dynamics Investigation of Ligand Access Channels and Mechanisms. *J. Mol. Biol.* **2000**, *303*, 797–811.

(22) Laio, A.; Parrinello, M. Escaping Free-Energy Minima. *Proc. Natl. Acad. Sci. U.S.A.* **2002**, *99*, 12562–12566.